THE JOURNAL OF PHYSICAL CHEMISTRY C

Article

High Photoresponsivity in Graphene Nanoribbon Field Effect Transistor Devices Contacted With Graphene Electrodes

Andrea Candini, Leonardo Martini, Zongping Chen, Neeraj Mishra, Domenica Convertino, Camilla Coletti, Akimitsu Narita, Xinliang Feng, Klaus Müllen, and Marco Affronte

J. Phys. Chem. C, **Just Accepted Manuscript** • Publication Date (Web): 21 Apr 2017

ACS Publications

The Journal of Physical Chemistry C is published by the American Chemical Society. 1155 Sixteenth Street N.W., Washington, DC 20036

High Photoresponsivity in Graphene Nanoribbon Field Effect Transistor Devices Contacted with Graphene Electrodes

Andrea Candini[1], Leonardo Martini[1,2], Zongping Chen[3], Neeraj Mishra[4], Domenica Convertino[4], Camilla Coletti[4], Akimitsu Narita[3], Xinliang Feng[5], Klaus Müllen[3] and Marco Affronte[2,1]*

[1]Centro S3, Istituto Nanoscienze - CNR, via G. Campi 213/A , 41125 Modena. Italy.

[2]Dipartimento di Scienze Fisiche, Matematiche e Informatiche, Università di Modena e Reggio Emilia via G. Campi 213/A , 41125/A Modena. Italy.

[3]Max Planck Institute for Polymer Research, Ackermannweg 10, D-55128 Mainz, Germany.

[4]Center for Nanotechnology Innovation @ NEST, Istituto Italiano di Tecnologia, Piazza San Silvestro 12, 56127 Pisa, Italy

[5]Center for Advancing Electronics Dresden (cfaed) & Department of Chemistry and Food Chemistry, Technische Universität Dresden, 01062 Dresden, Germany

KEYWORDS: graphene nanoribbons, graphene contacts, field-effect transistor, high sensitivity photodetector

ABSTRACT

Ultra-narrow graphene nanoribbons (GNRs) with atomically precise structures are considered a promising class of materials for the realization of optoelectronic and photonic devices with improved functionalities. Here we report the opto-electronic characterization of a field effect transistor devices made of a layer of bottom-up synthesized GNRs contacted with multilayer graphene electrodes, showing high photoresponsivity of 5×10^5 A/W for small incident power in the visible-UV range. Our results show that combining the properties of intrinsic graphene with that of semiconducting GNRs is a viable route to realize novel devices for optoelectronic and sensing applications.

1. INTRODUCTION

Graphene nanoribbons (GNRs) are narrow stripes of graphene, where quantum confinement induces a bandgap in the electronic structure, which can be precisely engineered by tailoring their size and morphology[1,2]. Although GNRs have been obtained by several techniques, including patterning of graphene[3] and unzipping of carbon nanotube[4,5], only bottom-up approaches, such as surface-assisted[6-9] and solution-mediated[10,11] synthesis, offer the degree of structural control needed to determine their optical and electronic properties. Particularly appealing is their integration in optoelectronics devices[12], to fully exploit the presence of a direct bandgap. In

addition, the appearance of novel features related to the GNR one-dimensional character has been predicted, including strong excitonic effects that may lead to enhanced light absorption and amplification[13-15]. However, optoelectronic devices made of bottom-up GNRs have so far been limited to a moderate light response[16], likely as a consequence of the relatively high series resistances of these devices, spoiling the intrinsic properties of the GNRs.

Graphene can be efficiently employed as transparent electrodes[17] and as the contact material for other low-dimensional systems, such as transition metal dichalcogenides[18-20]. In particular, so-called *all-graphene* devices have been recently proposed[21], suggesting that the graphene/GNR junction can be suitable to make good electrical contacts eventually leading to better performances than conventional semiconductor-metal devices. In this context, we have recently shown that the use of graphene electrodes to inject current in a layer of surface-synthesized chemical vapor deposition (CVD) -grown GNRs is suitable to realize short channel devices (100 - 200 nm) showing high ON-state currents and field-effect transistor (FET) behavior[9].

Here we demonstrate the sensitive phototransistor performances of our *all-graphene* devices, where the channel is made of a layer of structurally defined GNRs[9] and the source / drain electrodes are made of multilayer epitaxial graphene (MEG) grown on the C face of SiC[22]. The large optical bandgap of the GNRs (~1.8 eV) enables field-effect transistor (FET) operations as well as light absorption and photocurrent generation. Due to the good matching between the graphene electrodes and the flat layer of the CVD-grown GNRs[9], carriers and photo-generated carriers are efficiently extracted from the devices resulting in high current on/off ratios and enhanced photosensitivity. Our devices show a gate-tunable photocurrent with a photoresponsivity

approaching ~ 10^6 A/W in the broad visible-UV range for incident power below 1 pW. As a consequence the devices show the capability to detect signals down to the sub-fW range.

2. EXPERIMENTAL SECTION

2.1. Fabrication of the graphene electrodes. Multilayer epitaxial graphene devices were obtained on on-axis SiC(000-1) semi-insulating wafer dice following a previously reported procedure[23-24]. We determine an average thickness of 5 graphene layers by Raman spectroscopy (see Supporting Information Figure S1)[23,35]. The devices are realized by electron beam lithography, metal (Cr/Au) evaporation and oxygen plasma etching to pattern the device geometry and to realize the gap of about 100-200 nm. We remark that pristine graphene devices (described in the Supporting Information Figures S2-S4) show a very small gate dependence (< 10% of current modulation) with signature of ambipolar and no detectable light induced current.

2.2. GNR synthesis and transfer. Structurally defined chevron-type GNRs with well-defined edge structure (see inset of Figure 1a) have been grown from 6,11-dibromo-1,2,3,4-tetraphenyltriphenylene as the monomer by the ambient pressure CVD method under a mixture of Ar and H_2, following a reported procedure[9] on a gold/mica substrate. Briefly, in a horizontal tube furnace (Nabertherm, RT 80-250/11S), the monomer was sublimed at 250–325 °C with a heating belt (Thermocoax Isopad S20) onto the Au/mica substrate, which was maintained at 200–250 °C under gas flow of Ar (500 s.c.c.m.) and H_2 (100 s.c.c.m.). After heating at the same temperatures for another 5–30 min, the substrate was further annealed at 400–450 °C for 15 min. More details on the synthesis are given in Figures S5-S6 of the Supporting Information. The GNR layers have been comprehensively characterized through Raman spectroscopy, X-ray photoelectron

spectroscopy (XPS), high-resolution electron energy loss spectroscopy (HREELS) and scanning tunneling microscopy, which corroborated their high quality comparable to the GNRs fabricated under the UHV conditions[6,9].

The final devices are obtained by transfer the resulting GNR film on the pre-fabricated MEG electrodes without further fabrication (lithography) processes. The transfer process is performed according to the following procedure[9]: the sample is spin coated with a PMMA thin film as a mechanical support. The immersion in a hydrofluoric acid (HF) (40 wt. %) solution for several hours etch the mica away; after this step the samples are cleaned in ultrapure water; the gold film is removed by a commercial gold etchant (Sigma-Aldrich), leaving the GNR/PMMA film floating on water surface, which is then transferred on the new substrate with graphene electrodes. The PMMA film is finally removed with hot acetone and the sample is cleaned in isopropyl alcohol.

Figure 1b shows a scanning electron microscope (SEM) image of a typical device after fabrication.

2.3. Electrical characterization and measurements. All the electrical measurements have been realized in a 4-probe station (LakeShore PS-100) at the pressure of 10^{-4} torr. When not specified, the sample is kept at room temperature. The electrical characterization is performed with a Keithely 2636 source meter in the two-probes configuration. The illumination of the sample with white light is realized with a halogen lamp while for monochromatic light we employed a Quartz Tungsten Halogen lamp operated at up to 220 V and a diffraction grating monochromator working between 350 and 800 nm. In both cases, light is directed to the sample through a microscope 70x objective resulting in an uniform illuminated area. The incident light intensity is measured with a commercial Oriel photodiode over an area of $1cm^2$.

3. RESULTS AND DISCUSSIONS

3.1. Electrical characterization. Typical electrical characteristics of the devices are shown in Figure 2a,b. Measurements are performed at room temperature and under vacuum (10^{-4} torr), while the whole area of the device is illuminated by a white lamp. Figure 2a shows the transfer characteristics (source-drain current I_{sd} vs gate voltage V_g) for different bias (source-drain) voltages V_{sd}. The device displays an n-type semiconductor-like behavior, as also found for metal contacted GNRs[26], and the current saturates for positive gate voltages. The non-linear shape of the I_{sd}-V_{sd} characteristics shown for various V_g values (Figure 2b) and the asymmetry between negative and positive bias indicate non-Ohmic contacts, a common issue for bottom-up GNR devices[9,16,26]. We note the relatively high ON-state current value (I_{sd} > 10 nA for V_{sd} ~ 1 V) that we ascribe to the reduced contact resistance at the GNR/graphene interface[9]. This leads to a high ON/OFF current modulation up to ~10^4 for V_{sd} = -0.5 V.

3.2. Photoconductive properties. We now turn to the photoconductive properties of our devices. The light-dependence of the output current is described in Figure 3a, where the I_{sd}-V_{sd} characteristics with V_g = 0 V are presented with and without illumination (white lamp with measured intensity of 3.6 mW/cm^2 at 550 nm). The presence of light induces a strong increase in I_{sd}, doubling its value for V_{sd} > 1 V. The generated photocurrent ($I_{photo} = I_{light} - I_{dark}$) has a non-linear dependence on the source bias and can exceed several tens of nA, that is at least one order of magnitude more than previous GNR-based (with metallic electrodes) devices[16], for similar bias and incident illumination intensity. Figure 3b provides the dependence of the photocurrent on the gate voltage, where for each gate value the current is first measured under illumination and then

in the dark. We found that the photo-generated current is strongly gate dependent, which may be important for practical applications where an electrically tunable light-induced output is required. The illumination induces an increase of the current for all the gate values, except for large negative gate voltages (V_g < -30 V, i.e. when the device operates in the OFF state) where the light effect becomes negligible. The inset of Figure 2b displays the I_{light} / I_{dark} ratio which is always > 1 and for this particular sample was as a high as ~10 for V_g = -10 V. Interestingly, both I_{light} and I_{dark} saturate for the same gate voltage values, ruling out the photogating effect as the dominant mechanism at the origin of the observed behavior[27,28].

3.3. Photocurrent dependence on the incident power and wavelength. Further insights into the photoconductive behavior of the devices can be obtained by studying the dependence of the photocurrent on the photon wavelength λ and the incident power P_{inc} (Figure 4 a and b). The normalized photoresponsivity (i.e. the photocurrent divided by the incident power I_{photo} / P_{inc} normalized setting the value at 550 nm to 1) is given in Figure 4a for different incident photon wavelengths. The photoresponsivity is negligible for λ > 650-700 nm, and then it increases monotonously with decreasing λ without sign of saturation down to 380 nm. The onset at 650-700 nm corresponds to a photon energy of ~1.8 eV. The wavelength dependence of the photoresponsivity perfectly matches the UV-vis-NIR absorption spectra of the CVD-GNR films transferred on fused silica[9] (see also Figure S5b of the Supporting Information). These observations indicate that light-absorption by the GNRs is the most important mechanism for the photo-induced behavior, excluding other possible effects such as simple heating (see also Figure S8 of the Supporting Information). Figure 4b shows the dependence of the photocurrent on the illumination intensity. Here we employed a monochromatic light (λ = 550 nm) fixing V_{sd} and V_g

to 1 V and 0 V, respectively. Notably, a direct measurement of a signal as small as 10^{-3} W/m^2 was possible, demonstrating the high sensitivity of our devices. The photocurrent displays a sublinear behavior and tends to saturate when the light intensity is above 10 W/m^2.

Based on these observations, we propose a simple model for the operation of the devices as depicted in Figure 4c. Considering only the essential features of the device, the GNR film channel is schematically represented by the energy band structure of a homogenous semiconductor, and the MEG electrodes are represented by the band structure of one graphene layer[23,29]. To account for the non-linearity and the asymmetry of the I_{sd}-V_{sd} curves shown in Figure 2, we consider the presence of a Schottky-type barrier at the main interface between the GNR film and the graphene electrodes. The relatively high contact resistance can also explain the current saturation observed for $V_g > 0$ V, where the electric field is no longer effective in tuning the device intrinsic resistance[30]. Ohmic contacts with low resistances have been reported for MoS_2 devices[18-20] using monolayer graphene as the electrode, exploiting its electrically tunable workfunction. This effect is possibly masked in our devices by the use of multilayer graphene with weak gate dependence (Figure S4 of the Supporting Information). On the other hand, we can safely ascribe the observed field effects to the GNR film only.

When $V_g \geq 0$ V, the Fermi level of the MEG electrode is aligned with the conduction band of the GNRs and the current flows through the device upon the application of a bias voltage via thermoionic and tunnel effects (Figure 4c-left). Illuminating the sample with a light source of energy greater than the optical bandgap of the GNR film (1.8 eV) results in an increase of the current, because of the photo-induced generation of electron-hole pairs in addition to the promotion of carriers across the barrier (Figure 4c-center). Both mechanisms become more

efficient as the photon energy is increased, explaining the observed photocurrent dependence on λ. The extraction of the photo-generated carriers through the barrier is assisted by the application of a finite source-drain bias, resulting in the nonlinear dependence of I_{photo} versus V_{sd}. Lowering the gate voltage causes an increase of the interface barrier and the depopulation of the carrier in the GNR channel. When V_g < -30 V, the device is turned off and no current is flowing with or without illumination (Figure 4c-right). The sublinear dependence of I_{photo} versus incident power indicates a saturation of the available states for the photo-generated pairs and a decrease of the carrier extraction efficiency.

3.4. Estimation of the photoresponsivity. We now proceed to the quantitative evaluation of the light response of our devices. One of the most important parameters for a photosensitive device is its external photoresponsivity R defined as the ratio between the photo-induced current and the incident light power. To determine P_{inc} we need to estimate the device active area, which in our case is given by the GNR layer channel plus the contacts region with the multilayer graphene electrodes. Taking into account that no measurable light induced signal was observed in the pristine multilayer graphene (see Supporting Information Figure S3), we estimate as an upper limit of the device active area the square of 1μm × 1μm shown in Figure 1b. This leads to the calculated R given in Figure 5a as a function of the incident power. The photoresponsivity increases as the incident power is reduced, and at low incident power (< 10^{-14} W) the device possesses a remarkably high photoresponsivity of ~5 × 10^5 A/W, fixing the bias and gate voltage at 1 V and 0 V, respectively. To estimate the sensitivity of our device, i.e. the noise equivalent power (NEP), we measured the current noise in the dark state, fixing V_g = -10 V (where the I_{light} / I_{dark} ratio is maximum), and found that it is possible to detect illumination signals as small as ~ 1 × 10^{-16} W

with a bandwidth of 1 Hz (see Supporting Information Figure S9 for additional details). This translates to a specific detectivity $D^* \sim 10^{12}$ Jones (cm $Hz^{1/2}$ W^{-1}).

This high value for the photoresponsivity of our devices is another indication that the photocurrent is originated by the GNR film, since the maximum value reported for pristine graphene is 8 orders of magnitude lower[31]. Efficient mechanisms for light absorption and current multiplication have been predicted for ultra-small GNRs[13-15,32]. However, the key ingredient of our architecture is the use of graphene electrodes, resulting in a more efficient current injection/extraction with respect to previously reported GNRs-based devices employing metal electrodes[16]. Also the fact that the contact regions are directly exposed to the incoming light (and not below electrodes of thickness of several tens of nanometer) certainly plays an important role in the increased responsivity. Finally, it is worth to stress the use of a film of flatly lying GNRs grown by a surface-assisted method[9], avoiding their aggregation, to maximize the interaction with the electrodes and obtain good electrical contacts.

Time dependence of the photocurrent. In Figure 5b we present the time-resolved measurements of the photocurrent, by showing the temporal evolution of the drain current when switching on and off the light source. We found that the current has a rise time of typically ~ 25 ms and decays back to the original value in ~ 75 ms after the light is turned off. Our results can be interpreted by considering the presence of charged defects, which trap the photo induced holes allowing for the extraction of multiple electrons for every incident photon thus contributing to the photocurrent, further enhancing the sensitivity of the devices. When the light is switched off, the carriers are released back to the circuit and the current decays back to the initial value at timescales which depend on the characteristic lifetimes of these long-lived states. Our response times are in

line with other reported low-dimensional devices, where the presence of trap states contributes to the gain mechanism, showing typical timescales in the range 10 ms - 1 s[27,33-34].

The presence of charge traps can explain the saturating behavior of the responsivity shown in Figure 5a, since increasing the incident power leads to the saturation of these long-lived states, and a consequent decrease of the photodetection efficiency and responsivity. A further indication of the presence of defect states is suggested by the observation of slow relaxation times in the I_{ds} *vs* V_g measurements when the device is not illuminated, which is shown in the Supporting Information (Figure S12). The defects may be present in the substrate or the device itself, most likely at the ribbon-ribbon and ribbon-graphene junctions. For the sake of completeness, in the Supporting Information (Section 6, Figures S10 and S11) we present another device showing similar photoresponsivity but slower response times. This suggests that different types of defects, with different lifetimes, may be present, presumably originated from the fabrication and transfer processes. Admittedly, while the sensitivity of our devices compares well even with state-of-the-art semiconductors devices (for comparison, commercial Si-based photodetectors have a NEP of $\sim 10^{-14}$ W/Hz$^{-1/2}$ [35]) the relatively slow response time may limit their practical applications. Nevertheless, usage in applications where high sensitivity is desired even at the expense of a fast response time can be envisaged. Further device engineering will lead to improved fabrication and lower defects density, in order to achieve faster photodetection. For instance, considerable improvement can be obtained by adopting the clean transfer techniques developed for the van der Waals heterostructures[36,37].

4. CONCLUSIONS

To summarize, we presented a novel type of phototransistor device, made of bottom-up CVD-grown GNRs as the channel material and multilayer graphene as the electrodes. Our findings show the possibility to realize opto-electronic platforms fully based on graphene-based materials, where elements with different functionalities are integrated. GNR-based devices, with the chance of precisely tailoring their properties by modulating the monomer structures, hold great promise for the next generation of nano opto-electronics devices, in particular in fields where high light sensitivity is required.

FIGURES

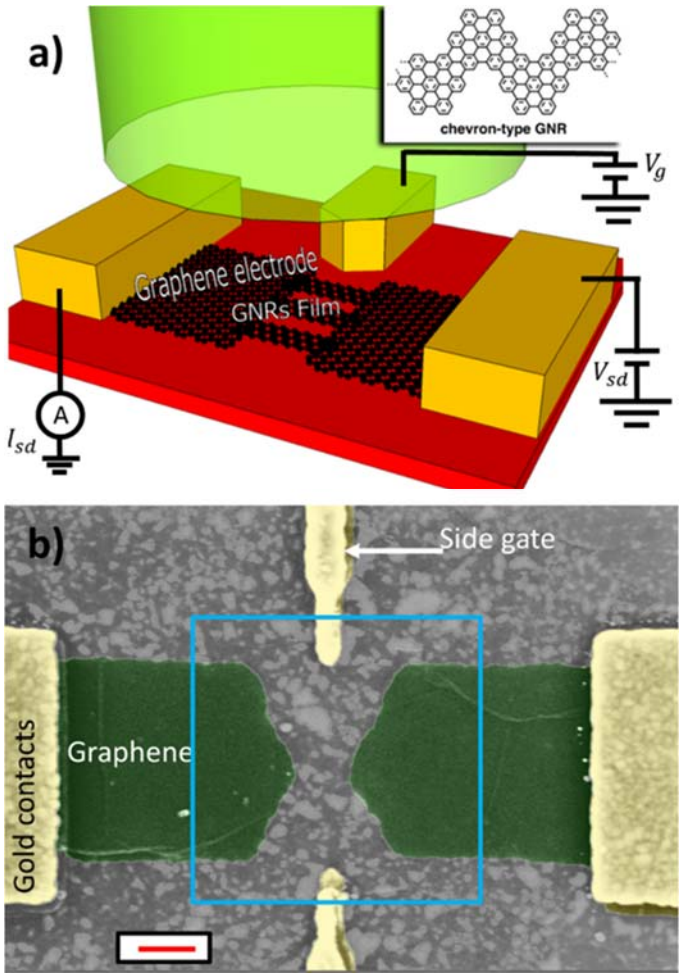

Figure 1. a) Schematic view and b) false-colour SEM image of a device made of the graphene nanoribbon channel (not visible at the SEM) and multilayer epitaxial graphene electrodes, grown on the C-face of SiC. Graphene = green; metal (Cr/Au) electrodes and lateral gate = (yellow); The inhomogeneities present in the substrate are a product of the GNRs transfer process. The scale bar is 200 nm.

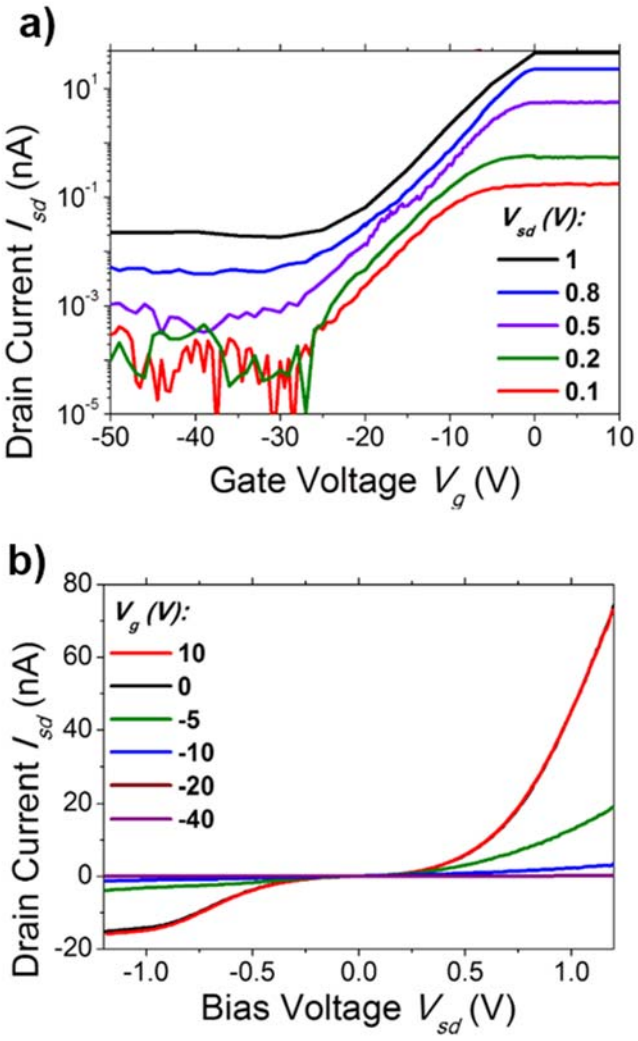

Figure 2. Room-temperature field-effect transistor characteristics, measured under illumination with a white lamp and in vacuum (10^{-4} torr). a) Gate voltage dependence of the current shown for various bias voltages. b) Corresponding I_{sd}-V_{sd} characteristics shown for different gate voltages.

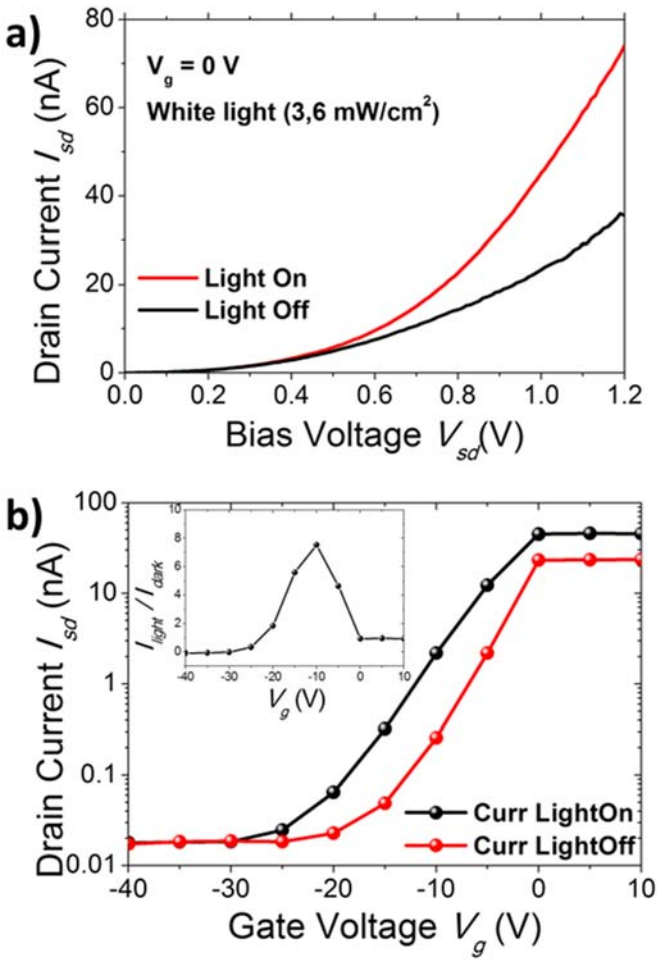

Figure 3. a) Current output characteristics of the device with and without illumination with a white lamp (power of 3.6 mW cm^{-2} measured at λ = 550 nm). b) Gate voltage dependence of the photocurrent as shown in (a) fixing the bias voltage at 1 V. For each point, the current is measured firstly under illumination (I_{light}), then the light is switched off (I_{dark}). The insert shows the ratio between the two measured values for each gate point.

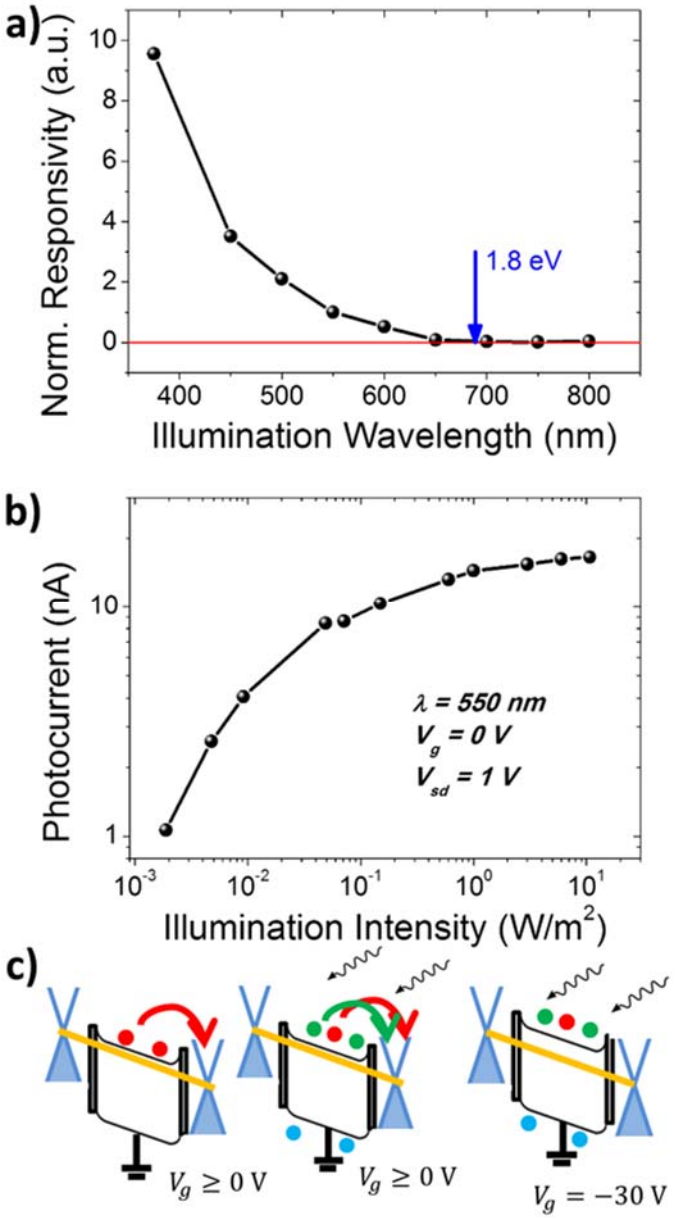

Figure 4. a) Normalized photoresponsivity (I_{photo} / P_{inc} = (I_{light} - I_{dark})/P_{inc}, setting the value at λ = 550 nm equal to 1) of the device as a function of the photon wavelength λ. b) Photocurrent versus light intensity at a fixed bias voltage of 1 V and gate voltage of 0 V, with λ = 550 nm. (c) Schematic model for the functioning of the GNR devices with graphene electrodes: the right panel represents the ON state ($V_g \geq 0$ V and finite V_{sd}) in the dark. In the central and right panels a light source of energy larger than the GNRs bandgap illuminate the sample. In the central panel

$V_g \geq 0$ V, while in the right panel the device is in the OFF state (V_g < -30 V). Red balls are the intrinsic carriers in the GNR channel, green-blue balls are the photogenerated electron-hole pairs.

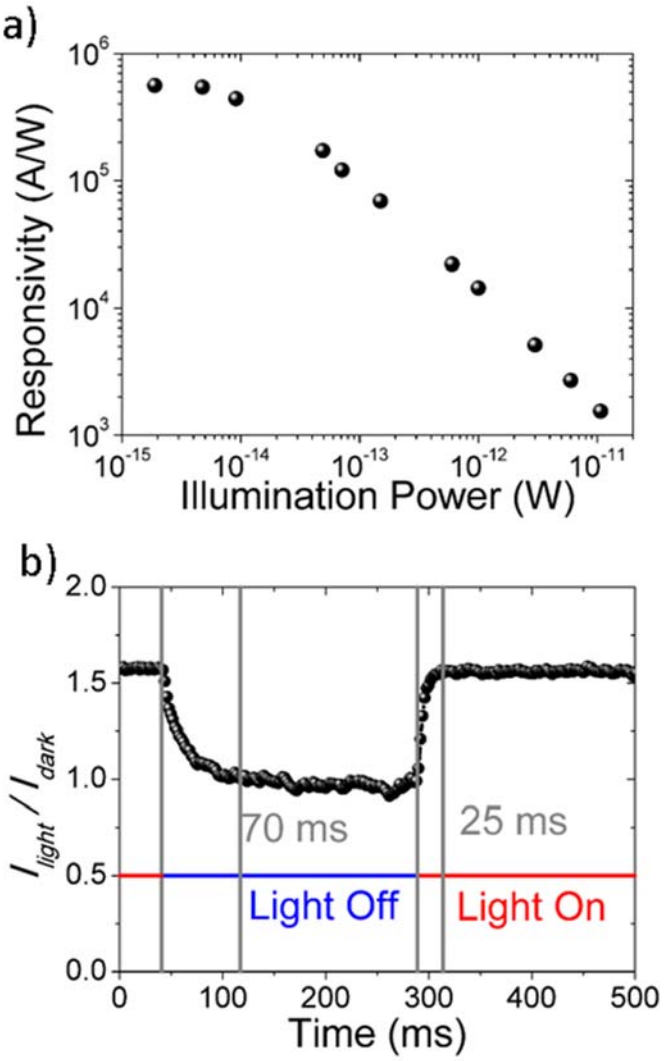

Figure 5. a) Photoresponsivity of the device under monochromatic illumination (λ = 550nm) for different incidence power values. This is calculated considering an active area equal to 1 × 1 μm² as shown in Figure 1(b). b) Time-resolved photocurrent of the device, measured fixing the source-drain bias voltage to 1 V and the gate voltage to 0 V. The illumination is provided by a white lamp (P ~ 0.5 × 10^{-12} W). The rise and fall times are indicated as the time needed to reach 95% of the steady state value.

ASSOCIATED CONTENT

Supporting Information.

The Supporting Information is available free of charge via the Internet at http://pubs.acs.org. Scheme of the CVD synthesis of the GNRs and absorption measurement. Characterization of the pristine graphene devices (without gap and before the GNR transfer). Raman characterization of the GNRs after the transfer on the multilayer graphene electrodes. Additional electrical characterization for the device presented in the main text and other devices with similar characteristics. Evaluation of the noise equivalent power.

AUTHOR INFORMATION

Corresponding Author

*andrea.candini@nano.cnr.it Phone: +39 059 2058376

Note

The authors declare no competing financial interest.

ACKNOWLEDGMENT

This work has been partially supported by the Italian Ministry for Research (MIUR) through the Futuro In Ricerca (FIR) grant RBFR13YKWX, by the European Community through the FET-Proactive Project “MoQuaS”, contract N.610449, by the European Union’s Horizon 2020 research and innovation programme under grant agreement No. 696656 – GrapheneCore1, by the DFG Priority Program SPP 1459 and by the Office of Naval Research BRC Program. We thank

F. Carillo and P. Pingue for support for the sample fabrication and the access to the nanofabrication facility of the Laboratorio NEST, Scuola Normale Superiore, Pisa, Italy.

REFERENCES

1. Castro Neto, A. H.; Guinea, F.; Peres, N. M. R.; Novoselov, K. S.; Geim, A. K. The electronic properties of graphene. *Rev. Mod. Phys.* **2009,** *81,* 109.

2. Yang, L.; Park, C.H.; Son, Y.W.; Cohen, M.L.; Louie, S.G. Quasiparticle energies and band gaps in graphene nanoribbons. *Phys. Rev. Lett.* **2007,** *99,* 186801.

3. Han, M.Y.; Ozyilmaz, B.; Zhang, Y.; Kim, P. Energy band-gap engineering of graphene nanoribbons. *Phys. Rev. Lett.* **2007,** *98,* 206805.

4. Jiao, L.Y.; Zhang, L.; Wang, X.R.; Diankov, G.; Dai, H.J. Narrow graphene nanoribbons from carbon nanotubes. *Nature* **2009,** *458,* 877-880.

5. Kosynkin, D.V. ; et al. Longitudinal unzipping of carbon nanotubes to form graphene nanoribbons. *Nature* **2009,** *458,* 872-876.

6. Cai, J.M.; et al. Atomically precise bottom-up fabrication of graphene nanoribbons. *Nature* **2010,** *466,* 470-473.

7. Cai, J.M. ; et al. Graphene nanoribbon heterojunctions. *Nature Nanotech.* **2014,** *9,* 896-900.

8. Chen, Y.C. ; et al. Molecular bandgap engineering of bottom-up synthesized graphene nanoribbon heterojunctions. *Nature Nanotech.* **2015,** *10,* 156-160.

9. Chen, Z.; Zhang, W.; Wang, X.-Y.; Palma, C.-A.; Lodi Rizzini, A.; Liu, B.; Abbas, A.; Richter, N.; Martini, L.; Berger, R.; Klappenberger, F.; Mishra, N.; Coletti, C.; Kläui, M.; Candini, A.; Affronte, M.; Zhou, C.; De Renzi, V.; del Pennino, U.; Barth, J. V. Räder, H. J.; Narita, A.; Feng, X.; Müllen, K. Synthesis of Graphene Nanoribbons by Ambient-Pressure Chemical Vapor Deposition and Device Integration. *J. Am. Chem. Soc.* **2016,** *138,* 15488–15496.

10. Schwab, M.G. ; et al. Structurally defined graphene nanoribbons with high lateral extension. *J. Am. Chem. Soc.* **2012,** *134,* 18169-18172.

11. Narita, A.; et al. Synthesis of structurally well-defined and liquid-phase-processable graphene nanoribbons. *Nature Chem.* **2014,** *6,* 126-132.

12. Bonaccorso, F.; Sun, Z.; Hasan, T.; Ferrari, A. C. Graphene photonics and optoelectronics. *Nature Photon.* **2010,** *4,* 611 - 622.

13. Yang, L.; Cohen, M. L.; Louie, S. G. Excitonic effects in the optical spectra of graphene nanoribbons. *Nano Lett.* **2007,** *7,* 3112–3115.

14. Prezzi, D.; Varsano, D.; Ruini, A.; Marini, A.; Molinari, E. Optical properties of graphene nanoribbons: The role of many-body effects. *Phys. Rev. B* **2008,** *77,* 041404.

15. Denk, R.; et al. Exciton-dominated optical response of ultra-narrow graphene nanoribbons. *Nature Commun.* **2014,** *5,* 4253.

16. Sakaguchi, H.; Kawagoe, Y.; Hirano, Y.; Iruka, T.; Yano, M.; Nakae, T. Width-Controlled Sub-Nanometer Graphene Nanoribbon Films Synthesized by Radical-Polymerized Chemical Vapor Deposition. *Adv. Mater.* **2014,** *26,* 4134–4138.

17. Kim, K. S.; et al. Large-scale pattern growth of graphene films for stretchable transparent electrodes. *Nature* **2009,** *457,* 706–710.

18. Yu, L.; et al. Graphene/MoS_2 hybrid technology for large-scale two-dimensional electronics. *Nano Lett.* **2014,** *14,* 3055–3063.

19. Cui, X.; et al. Multi-terminal transport measurements of MoS_2 using a van der Waals heterostructure device platform. *Nature Nanotech.* **2015,** *10,* 534–540.

20. Lui, Y.; et al. Toward barrier free contact to Molybdenum Disulfide using graphene electrodes. *Nano Lett.* **2015,** *15,* 3030-3034.

21. Kang, J.; Sarkar, D.; Khatami, Y.; Banerjee, K. Proposal for all-graphene monolithic logic circuits. *Appl. Phys. Lett.* **2013,** *103,* 083113.

22. Berger, C.; Song, Z.; Li, X.; Wu, X.; Brown, N.; Naud, C.; Mayou, D.; Li, T.; Hass, J.; Marchenkov, A. N.; Conrad, E. H.; First, P. N.; de Heer, W. A.; Electronic Confinement and Coherence in Patterned Epitaxial Graphene. *Science* **2006,** *312,* 1191-1196.

23. Convertino, D.; Rossi, A.; Miseikis, V.; Piazza, V.; Coletti, C. Thermal decomposition and chemical vapor deposition: a comparative study of multi-layer growth of graphene on SiC(000-1). *MRS Advances* **2016,** *1,* 3667-3672.

24. Candini, A.; et al. Electroburning of few-layer graphene flakes, epitaxial graphene, and turbostratic graphene discs in air and under vacuum. *Beilstein J. of Nanotech.* **2015,** *6,* 711-719.

25. Shivaraman, S.; Chandrashekhar, M. V. S.; Boeckl, J. J.; Spencer, M. G. Thickness Estimation of Epitaxial Graphene on SiC Using Attenuation of Substrate Raman Intensity. *J. Electron. Mater.* **2009,** *38,* 725-730.

26. Bennett, P. B. ; et al. Bottom-up graphene nanoribbon field-effect transistors. *Appl. Phys. Lett.* **2013,** *103,* 253114.

27. Konstantatos, G.; et al. Hybrid graphene–quantum dot phototransistors with ultrahigh gain. *Nature Nanotechnol.* **2012,** *7,* 363–368.

28. Koppens, F. H. L.; Mueller, T.; Avouris, Ph.; Ferrari, A. C.; Vitiello, M. S.; Polini, M. Photodetectors based on graphene, other two-dimensional materials and hybrid systems. *Nature Nanotech.* **2014,** *9,* 780-793.

29. Hicks, J. ; Shepperd, K. ; Wang, F. ; Conrad, E. H. The structure of graphene grown on the SiC (000-1) surface *J. Phys. D : Appl. Phys.* **2012,** *45,* 154002.

30. Lui, R.; et al. Gate Modulation of Graphene-ZnO Nanowire Schottky Diode. *Sci. Rep.* **2015,** *5,* 10125.

31. Mueller, T.; Xia, F.; Avouris, P. Graphene photodetectors for high-speed optical communications. *Nature Photon.* **2010,** *4,* 297–301.

32. Soavi, G.; et al. Exciton–exciton annihilation and biexciton stimulated emission in graphene nanoribbons. *Nat. Commun.* **2016,** *7,* 11010.

33. Lopez-Sanchez, O.; Lembke, D.; Kayci, M.; Radenovic, A.; Kis, A. Ultrasensitive photodetectors based on monolayer MoS2. *Nature Nanotech.* **2013,** *8,* 497–501.

34. Island, J. O.; Blanter, S. I.; Buscema, M.; van der Zant, H. S. J.; Castellanos-Gomez, A. Gate Controlled Photocurrent Generation Mechanisms in High-Gain In_2Se_3 Phototransistors. *Nano Lett.* **2015,** *15,* 7853-7858.

35. Krainak, M. A.; Sun, X.; Yang, G.; Lu, W. Comparison of linear-mode avalanche photodiode lidar receivers for use at one-micron wavelength. *Proc. SPIE* **2010,** *7681,* 76810Y.

36. Geim, A. K.; Grigoreva, I. V. Van der Waals heterostructures. *Nature* **2013,** *499,* 419-425.

37. Castellanos-Gomez, A.; Buscema, M.; Molenaar, R.; Singh, V.; Janssen, L.; van der Zant, H. S. J.; Steele, G. A. Deterministic transfer of two-dimensional materials by all-dry viscoelastic stamping. *2D Mater.* **2014,** *1,* 011002.

Insert Table of Contents Graphic and Synopsis Here